ELSEVIER

Contents lists available at ScienceDirect

Fundamental Plasma Physics

journal homepage: www.elsevier.com/locate/fpp





Radiative damping of toroidal Alfvén eigenmode in low-shear plasmas

B.N. Breizman ^a, S.E. Sharapov ^{b,*}

- ^a Institute for Fusion Studies, The University of Texas, Austin, TX 78712, United States
- ^b United Kingdom Atomic Energy Authority, Culham Campus, Abingdon, Oxfordshire OX14 3DB, UK

ARTICLE INFO

Keywords:
Toroidal Alfven eigenmode
Kinetic Alfven wave
Radiative damping
Non-ideal effect
Tokamak
Magnetic shear
Magnetic fusion
Alpha-particle driven instability

ABSTRACT

Instabilities of Alfvén eigenmodes (AEs) are of significant concern because they can enhance the cross-field transport of fusion-born alpha particles beyond the neoclassical level in magnetic fusion plasmas. The threshold value of alpha-particle pressure for exciting AEs depends critically on the damping rate of AEs. The damping mechanisms include kinetic damping due to interactions with thermal particles, continuum damping due to AE frequency crossing Alfvén continuum, and radiative damping due to emitting kinetic Alfvén waves (KAWs). The radiative damping is substantial and can even prevail in high-temperature burning plasmas [1]. We revisit the radiative damping analytic theory for TAE in plasmas with low positive magnetic shear, considering TAE with an eigenfrequency near the bottom of TAE-gap and with poloidal harmonics of the same sign (even TAE). In contrast to earlier papers, we provide the damping calculations in real space rather than Fourier space. This approach is straightforward technically and more enlightening from a physics standpoint for benchmarking numerical calculations of radiative damping. The parametric dependence of the resulting damping rate agrees with that of Refs. [2-5], but it has a smaller numerical factor in front of it.

Introduction

Magnetic fusion research has now reached the point at which burning thermonuclear plasma becomes possible with significant populations of fusion-born alpha particles. Consequently, there is a need to assess collective phenomena that may affect alpha-particle confinement. Excitation of weakly-damped Alfvén eigenmodes (AEs) is of particular concern because they can enhance alpha particle transport far beyond the neoclassical level. The threshold value of alpha-particle pressure for exciting AEs depends critically on the damping rate of AEs. There are three main damping mechanisms of AEs: (1) their interaction with thermal electrons and ions, (2) coupling of Alfvén eigenmodes to the Alfvén continuum, and (3) transformation of Alfvén eigenmodes into kinetic Alfvén waves (KAW). The last process, dubbed radiative damping, will likely dominate in high-temperature plasmas of ITER [1]. From the theory standpoint, the damping mechanisms are tractable individually. The goal of this paper is to revisit the radiative damping.

We present a technique that is more compact and transparent than the past rather intricate calculations of the radiative damping rate in Refs [2–5], where the authors used either ballooning approximation [2, 3] or Fourier-transformed basic equations with the WKB-approximation in Fourier space [4,5]. In contrast, we use a real-space formalism, in

which the Alfvén eigenmode represents a smooth radially localized source that emits the short wavelengths kinetic Alfvén waves. The WKB approximation then applies only to the emitted wave rather than to the total field of the Alfvén eigenmode and KAW. Similar to Refs. [2–5], the separation of spatial scales between the AE and KAW makes the radiative losses depend on this separation exponentially. However, we find that the pre-exponential numerical factor differs from that of Refs. [2,5].

To be specific, we consider Toroidal Alfvén Eigenmode (TAE) in a large aspect ratio tokamak (ε <1) with circular magnetic surfaces in the limit of large mode numbers and low magnetic shear (S<1) [6]. TAEs are known to reside within gaps in the Alfvén continuum frequency spectrum. The gap accommodates multiple TAEs when $S < \varepsilon$ [7]. However, there is only one TAE per gap when $S > \varepsilon$, which we assume here to be the case. The frequency of that mode is only slightly above the lower tip of the TAE-gap, and the mode radial width is much smaller than the distance between the neighboring gaps. Because of that, the mode is tractable within a single-gap approximation. Such a mode has only two poloidal components, and the mode frequency is real in the ideal MHD limit.

The TAE radiative damping is due to two nonideal effects (finite ion Larmor radius and finite parallel electric field). These effects couple TAE to kinetic Alfvén waves (KAW) described by the following dispersion

E-mail address: Sergei.Sharapov@ukaea.uk (S.E. Sharapov).

https://doi.org/10.1016/j.fpp.2025.100086

^{*} Corresponding author.

relation [8]:

$$\omega^{2} = k_{\parallel m}^{2} V_{A}^{2} \left(1 + k_{\perp}^{2} \rho_{i}^{2} \left(\frac{3}{4} + \frac{T_{e}}{T_{i}} \right) \right). \tag{1}$$

Here, $k_{\perp}^2=k_r^2+k_{\theta}^2$, $\rho_i^2=\frac{2T_i}{m_i\omega_{Bl}^2}$ is square of thermal ion Larmor radius, and the parallel wave-vector of the m-th harmonic with toroidal mode number n has a radial dependence determined by the safety factor $q(r)=rB_{\mathcal{E}}/RB_{\theta}$:

$$k_{\parallel m}(r) = \frac{1}{R} \left(n - \frac{m}{q(r)} \right). \tag{2}$$

Unlike ideal shear Alfvén waves (including ideal TAE), the kinetic Alfvén waves have a non-zero radial group velocity and, therefore, propagate across the field. These outgoing KAWs, coupled to TAE, take away some TAE energy thus causing the TAE "radiative damping".

To explain the coupling between TAE and KAW, we consider Fig. 1 showing Alfvén continuum for two toroidally coupled poloidal harmonics, and the regions of KAW propagation. First, Fig. 1 shows schematically which ways the cross-field KAW energy flux can go. The sign "+" in front of the finite Larmor radius term in (1) tells us that KAW with poloidal mode number m can only exist and propagate *above* the Alfvén continuum curve with the same m. The propagation areas of KAWs emitted at the TAE frequency are shown in grey in Fig. 1. There are two different areas in the vicinity of a TAE-gap: one for KAW with mode number m and the other – for KAW with mode number m-1.

Basic equations and separation of scales

In contrast to cylindrical geometry, where there is no linear coupling between shear Alfven modes with different azimuthal numbers, the poloidal components of the mode become coupled in a torus. Most of the coupling is between the neighboring poloidal components. As a result, in the limit of low shear and large aspect ratio, each eigenmode involves predominantly two poloidal components. The coupling creates gaps in the Alfvén continuum where the discrete Toroidal Alfven Eigenmodes reside.

The gaps form where the local frequencies coincide for the cylindrical Shear Alfven modes with the poloidal mode numbers m and m-1 and the same toroidal number n, i.e., $\omega=-k_{\parallel m}(r_m)V_A(r_m)=k_{\parallel m-1}(r_m)V_A(r_m)$, where $k_{\parallel m}(r)=[n-m/q(r)]/R$ is the component of the wave vector parallel to the magnetic field, V_A is the Alfven velocity, and R is the tokamak major radius. The safety factor at the gap location $(r=r_m)$ is

$$q(r_m) = \left(m - \frac{1}{2}\right) / n. \tag{3}$$

For every poloidal harmonic m there is also a location $r=r_{m-1}$ where that harmonic couples to its lower sideband m-1. The distance between the surfaces $r=r_m$ and $r=r_{m-1}$ depends on the magnetic shear S=(r/q)dq/dr and can be estimated as

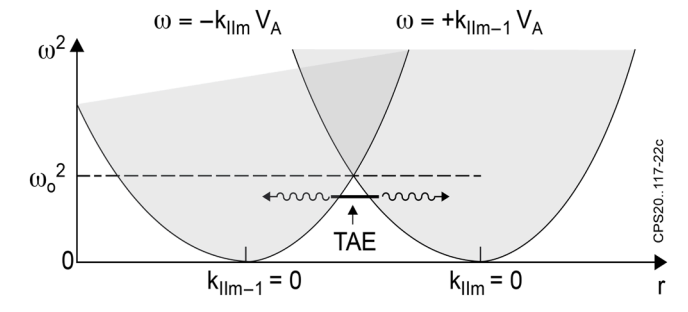


Fig. 1. Radial structure of toroidal Alfvén continuum with poloidal harmonics m and m-1 (same *n*) and the areas of propagation of KAWs with harmonics m and m-1 (shaded areas).

$$|r_m - r_{m-1}| \sim r_m/(nqS). \tag{4}$$

Because of the low shear, this distance exceeds the width of the mode significantly, which justifies the neglect of the m+1 component in our analysis. In other words, we treat TAE within a 'single-gap' approximation. In addition, we assume that plasma pressure is negligibly small and that the equilibrium magnetic field has circular flux surfaces.

The radiative damping of the TAE mode is associated with kinetic contributions (non-ideal corrections) to the equations for the two coupled poloidal components of the mode (φ_m and φ_{m-1}). These contributions are due to the finite ion Larmor radius and finite parallel electric field. They introduce fourth order radial derivatives in the governing equations [9,10,6]:

$$\rho^2 \frac{d^4}{dr^4} \varphi_m + L_m \varphi_m + \frac{\widehat{\varepsilon}}{4a^2 R^2} \frac{d^2}{dr^2} \varphi_{m-1} = 0$$
 (5)

$$\rho^2 \frac{d^4}{dr^4} \varphi_{m-1} + L_{m-1} \varphi_{m-1} + \frac{\widehat{\varepsilon}}{4q^2 R^2} \frac{d^2}{dr^2} \varphi_m = 0$$
 (6)

Here, the toroidicity coupling coefficient is $\widehat{\varepsilon} \equiv (5/2)(r/R)$, the differential operator L_m is defined as

$$L_m \varphi_m \equiv \frac{d}{dr} \left(\frac{\omega^2}{V_A^2} - k_{\parallel m}^2 \right) \frac{d\varphi_m}{dr} - \frac{m^2}{r^2} \left(\frac{\omega^2}{V_A^2} - k_{\parallel m}^2 \right) \varphi_m \tag{7}$$

and the non-ideal parameter is

$$\rho^2 \equiv \frac{1}{\left(2qR\right)^2} \frac{T_i}{m_i \omega_{Bi}^2} \cdot \left(\frac{3}{4} + \frac{T_e}{T_i}\right).$$

Without the non-ideal terms, Eqs. (5), (6) involve two very different radial scales as Fig. 2 shows. The outer scale $\Delta^{out} = r_m/m$ characterizes the uncoupled cylindrical harmonics φ_m and φ_{m-1} away from the gap (but still not as far as the upper sideband coupling location r_{m+1}), whereas the inner scale $\Delta^{in} = \frac{er_m}{m} \ll \Delta^{out}$ refers to the close vicinity of the TAE-gap where there is strong toroidal coupling between φ_m and φ_{m-1} .

The non-ideal contributions (fourth order radial derivatives) are essential only within the narrow inner scale, where it is allowable to ignore the non-derivative terms in Eqs (5) and (6). With this simplification, we find that the mode equations can be integrated twice and

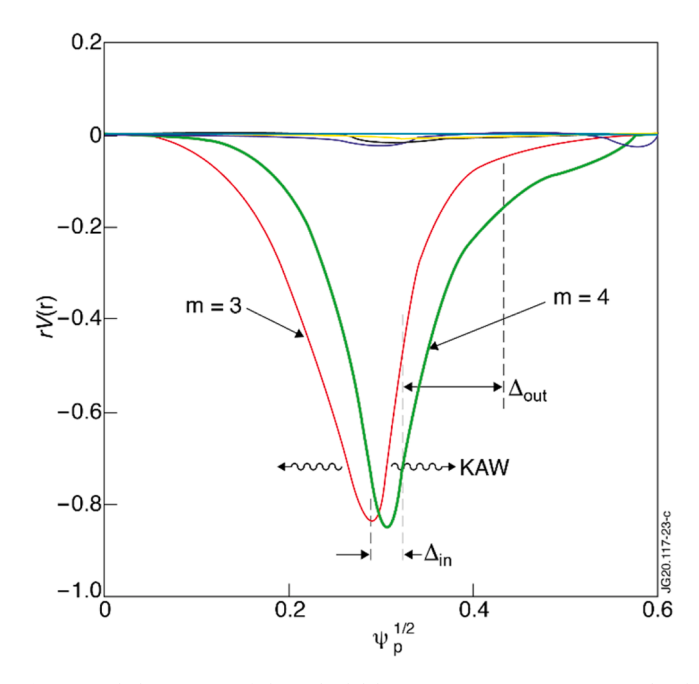


Fig. 2. Radial structure of the poloidal harmonics in even TAE: normalized perturbed plasma velocity versus r/a.

reduced to [10]

$$\lambda^2 U'' + (g+z)U + V = C_m, \tag{8}$$

$$\lambda^2 V'' + (g - z)V + U = -C_{m-1}, \tag{9}$$

where C_m and C_{m-1} are the integration constants.

We herein use the following notations:

$$\begin{split} U &\equiv \frac{\partial \varphi_m}{\partial z} \\ V &\equiv \frac{\partial \varphi_{m-1}}{\partial z} \\ z &= 4n[q(r) - q_m]/\widehat{\varepsilon} \\ g &\equiv (\omega^2 - \omega_0^2)/\widehat{\varepsilon}\omega_0^2 \\ \omega_0(r_m) &= \frac{V_A}{2\sigma R} \end{split} \tag{10}$$

$$\lambda^2 = (4/\widehat{\varepsilon})^3 \frac{m^2 S^2}{4r_m^2} \frac{T_i}{m_i \omega_{Ri}^2} \left[\frac{3}{4} + \frac{T_e}{T_i} \right] \ll 1$$

At this point, it is instructive to mention two essential features of TAE in the low shear limit and for $\lambda=0$. First, the normalised eigenfrequency of TAE g is very close to -1 for this mode. More specifically,

$$g = -1 + \frac{\pi^2 S^2}{8}. (11)$$

Second, the TAE with eigenfrequency below the centre of the TAE-gap frequency ω_0 has two dominant poloidal harmonics of the same sign, i.e., this TAE has even parity [6] with

$$C_m = C_{m-1}. (12)$$

We will explain these features for completeness by reproducing their derivation in Ref [6]. We will then use them effectively in our calculation of radiative damping.

TAE structure for $\lambda = 0$

Eqs. (8) and (9) become algebraic for $\lambda=0$. This gives the following straightforward inner-layer solution for φ_m and φ_{m-1} :

$$\phi_m^{in} = -\frac{gC_m + C_{m-1}}{\sqrt{1 - g^2}} \tan^{-1} \frac{z}{\sqrt{1 - g^2}} + \frac{C_m}{2} \ln |z^2 + (1 - g^2)| + const, \qquad (13)$$

$$\varphi_{m-1}^{in} = \frac{gC_{m-1} + C_m}{\sqrt{1-g^2}} tan^{-1} \frac{z}{\sqrt{1-g^2}} + \frac{C_{m-1}}{2} ln \big| z^2 + \big(1-g^2\big) \big| + const. \quad (14)$$

As seen from Eqs. (13) and (14), φ_m and φ_{m-1} exhibit jumps at the ther inner layer, i.e.,

$$\Delta \varphi_m^{in} = -\pi \frac{gC_m + C_{m-1}}{\sqrt{1 - g^2}},\tag{15}$$

$$\Delta \varphi_{m-1}^{in} = \pi \frac{gC_{m-1} + C_m}{\sqrt{1 - g^2}},\tag{16}$$

These jumps must match the jumps in the outer solution of Eqs. (5) and (6) for φ_m and φ_{m-1} . Because there is no significant coupling between φ_m and φ_{m-1} in the outer area, one can ignore the small $\hat{\varepsilon}$ as well as ρ^2 there. By expanding $k_{\parallel m}(r)$ about the gap surface in the low-shear limit, we rewrite Eq. (5) in the following form:

$$\frac{d}{dx}x\frac{d\varphi_m}{dx} - x\frac{\varphi_m}{S^2} = x\frac{d\varphi_m}{dx},\tag{17}$$

where $x = nq(r) - m + \frac{1}{2}$. The term $x \frac{d\varphi_m}{dx}$ on the right-hand side of this equation can be treated as a perturbation. Thus, to lowest order, we neglect this term and write the solution of Eq. (17) as

$$\varphi_m^{out} = -C_m K_0(|x/S|) \tag{18}$$

where K_0 is the zeroth-order Macdonald function [11]. The integration constant C_m in Eq. (18) ensures that $\frac{d\varphi_m}{dr}$ matches the asymptotic solution of Eqs. (8) and (9).

We note that the lowest order outer solution is an even function of x. To find the odd correction to φ_m , we substitute Eq. (18) into the right-hand side of Eq. (17) and integrate Eq. (17) (with the boundary conditions $\varphi_m(-\infty) = \varphi_m(+\infty) = 0$. We then find that φ_m has a discontinuity at small values of x:

$$\left. \left. \varphi_m^{out} \right|_{x \to -0} - \left. \varphi_m^{out} \right|_{x \to +0} = C_m \frac{\pi^2 S}{4} \tag{19}$$

A similar procedure applied to φ_m 1 gives

$$\left. \varphi_{m-1}^{\text{out}} \right|_{x \to -0} - \left. \varphi_{m-1}^{\text{out}} \right|_{x \to +0} = -C_{m-1} \frac{\pi^2 S}{4}$$
 (20)

By matching Eqs. (19) and (20) to (15) and (16) we find the above-stated features (11) and (12).

Evaluation of radiative damping

The mode with $C_m = C_{m-1}$ and $g + 1 \ll 1$ is nearly symmetric, i.e.,

$$U+V>>U-V \tag{21}$$

It is thus convenient to rearrange Eqs. (8) and (9) to

$$\lambda^{2}(U+V)''+(g+1)(U+V)+z(U-V)=0 \tag{22}$$

$$\lambda^{2}(U-V)'' + (g-1)(U-V) + z(U+V) = 2C_{m}$$
(23)

By dropping off the first term in (23) and using (23) to express U-V via U+V in (22), we obtain

$$\lambda^{2}(U+V)''+(g+1)(U+V)+\frac{z^{2}}{2}(U+V)=C_{m}z \tag{24}$$

We now split U + V into $\widetilde{F} + F_0$, i.e.,

$$U + V = \widetilde{F} + F_0 \tag{25}$$

where

$$F_0 = \frac{2C_m z}{z^2 + 2g + 2} \tag{26}$$

is the TAE spatial structure, and \widetilde{F} is the radiated field to be calculated. We thus obtain the following inhomogeneous equation to solve:

$$\lambda^2 \widetilde{F}'' + (g+1)\widetilde{F} + \frac{z^2}{2} \widetilde{F} = -\lambda^2 F'_0$$
 (27)

We note that the reduction of Eqs. (22) and (23) to (27) differs from the earlier analysis of those equations in Refs. [2–5]. More specifically, in Refs. [2–5], those equations were Fourier transformed, taking advantage of the linear z-dependence in the coefficients, and were combined into a second-order differential equation in Fourier representation. The authors then used a WKB approach in Fourier space to solve the second-order equation with the ensuing need to interpret the WKB result at low wavenumbers, where the approximation is problematic. Our real-space derivation of Eq. (27) and its subsequent WKB solution is free from such vulnerability because we use the WKB approximation exclusively for the short-wavelength radiated field, for which the TAE provides a known spatially smooth source. It is then apparent that the radiation is exponentially small because its wavelength is much shorter than the width of the source.

We consider the following WKB fundumental solutions for homogenious Eq. (27):

$$\psi_{+} = \frac{1}{\sqrt{k}} \exp(i\Phi)$$

$$\psi_{-} = \frac{1}{\sqrt{k}} \exp(-i\Phi)$$

$$\Phi \equiv \int_{0}^{z} k dx$$

$$k \equiv \sqrt{\frac{g+1}{\lambda^{2}} + \frac{z^{2}}{2\lambda^{2}}}$$
(28)

The small value of λ ensures that these fundamental solutions have very short wavelenth.

The WKB-eigenfunctions ψ_+ and ψ_- represent the waves propagating in positive and negative directions, respectively. The inhomogeneous solution can then be written as

$$\widetilde{F} = -\frac{1}{(\psi'_{+}\psi_{-} - \psi'_{-}\psi_{+})} \left(\psi_{+} \int_{-\infty}^{z} F'_{0}\psi_{-}dz - \psi_{-} \int_{\infty}^{z} F''_{0}\psi_{+}dz \right)$$
(29)

or equivalently,

$$\widetilde{F} = \frac{i}{2} \left(\frac{1}{\sqrt{k}} \exp(i\Phi) \int_{-\infty}^{0} F^{\prime\prime}{}_{0} \exp(-i\Phi) \frac{dz}{\sqrt{k}} - \frac{1}{\sqrt{k}} \exp(-i\Phi) \int_{\infty}^{0} F^{\prime\prime}{}_{0} \exp(i\Phi) \frac{dz}{\sqrt{k}} \right)$$

$$+ \frac{i}{2} \left(\frac{1}{\sqrt{k}} \exp(i\Phi) \int_{0}^{z} F^{\prime\prime}{}_{0} \exp(-i\Phi) \frac{dz}{\sqrt{k}} - \frac{1}{\sqrt{k}} \exp(-i\Phi) \int_{0}^{z} F^{\prime\prime}{}_{0} \exp(i\Phi) \frac{dz}{\sqrt{k}} \right)$$

$$(30)$$

Taking into account expressions (19) and (20) for the jumps in the outer solution, we now have the following matching condition for the jumps of the inner and outer solutions in terms of F_0 and \widetilde{F} :

$$\int_{-\infty}^{\infty} (2C_m - zF_0 - z\widetilde{F})dz = \pi^2 SC_m$$
(31)

Without \widetilde{F} , this condition, together with (26), gives the TAE dispersion relation (11) with a real frequency.

We then need only the imaginary part of \widetilde{F} to calculate the radiative damping rate as a small imaginary part of the mode frequency. The imaginary part of \widetilde{F} comes entirely from the first-line terms in (30) so that

$$\operatorname{Im}\widetilde{F} = \frac{i}{2} \left(\frac{\sin\Phi(z)}{\sqrt{k(z)}} \int_{-\infty}^{\infty} F'_{0}(z') \frac{\sin\Phi(z')}{\sqrt{k(z')}} dz' \right). \tag{32}$$

We note that

$$F_0 = \frac{C_m z}{k^2 \lambda^2},\tag{33}$$

which transforms (32) to

$$\operatorname{Im}\widetilde{F} = -\frac{\operatorname{Ic}_{m}}{2\lambda^{2}} \left(\frac{\sin\Phi(z)}{\sqrt{k(z)}} \int_{-\infty}^{\infty} \frac{\sin\Phi(z')}{\sqrt{k(z')}} z' \, dz' \right) \tag{34}$$

via integrating by parts and keeping only the largest term (derivatives of Φ).

We now include \tilde{F} into (31) to obtain

$$g+1 = \frac{\pi^2 S^2}{8} + \frac{S}{4C_m} \operatorname{Im} \int_{-\infty}^{\infty} z \widetilde{F} dz$$

$$\left(\omega^2 - \omega_0^2\right) / \widehat{\varepsilon} \omega_0^2 + 1 = \frac{\pi^2 S^2}{8} \left\{ 1 - i \frac{a}{\pi} \left[\int_{-\infty}^{\infty} \frac{\sin \Phi(x)}{(1+x^2)^{1/4}} x dx \right]^2 \right\}$$
(35)

with $\omega = \omega_{\text{Real}} + i\gamma$.

This equation gives the following expression for the mode damping rate $(-\gamma)$:

$$-\frac{\gamma}{\omega_0} = \frac{\pi S^2 \widehat{\varepsilon}}{16} a \left[\int_{-\infty}^{\infty} \frac{\sin \Phi(x)}{(1+x^2)^{1/4}} x dx \right]^2, \tag{36}$$

where

$$a \equiv \frac{1 - g_{\omega = \omega_{\text{Red}}}^2}{\sqrt{2}\lambda} = \frac{\pi^2 S^2}{4\sqrt{2}\lambda} >> 1 \tag{37}$$

and

$$\Phi(x) \equiv a \int_{0}^{x} \sqrt{1 + y^2} dy. \tag{38}$$

In order to evaluate the exponentially small integral in Eq. (36), we introduce a new integration variable Z so that $x = \sinh z$. We then have

$$\int_{-\infty}^{\infty} \frac{\sin\Phi(x)}{(1+x^2)^{1/4}} x dx = 2\operatorname{Im} \int_{0}^{\infty} \exp\left[i\frac{a}{4}\sinh2z + i\frac{a}{2}z\right] (\cosh z)^{1/2} \sinh z dz$$
(39)

We note that the integral in Z along the imaginary axis from 0 to $i\pi/2$ is real, which allows us to shift the integration contour upward to $i\pi/2$, i. e., set $z=i\pi/2+t$ to obtain

$$\int_{-\infty}^{\infty} \frac{\sin\Phi(x)}{(1+x^2)^{1/4}} x dx = 2\operatorname{Im} \int_{0}^{\infty} \exp\left[-i\frac{a}{4} \sinh 2t + i\frac{a}{2}t - \frac{\pi a}{4}\right] (i\sinh t)^{1/2} i\cosh t dt$$
 (40)

At a >> 1, only small values of t contribute to this integral so that

$$\int_{-\infty}^{\infty} \frac{\sin\Phi(x)}{(1+x^2)^{1/4}} x dx = 2 \text{Im} \int_{0}^{\infty} \exp\left[-i\frac{a}{3}t^3 - \frac{\pi a}{4}\right] (it)^{1/2} i dt$$

$$= \frac{2}{3} \sqrt{\frac{3\pi}{a}} \exp\left[-\frac{\pi a}{4}\right]$$
(41)

We finally combine Eqs. (41) and (36) and (37) into

$$\begin{split} &-\frac{\gamma}{\omega_0} = \frac{\pi^2 S^2 \widehat{\varepsilon}}{12} \exp\left[-\frac{\pi a}{2}\right] \\ &a \equiv \frac{\pi^2 S^2}{4\sqrt{2}\lambda} >> 1 \\ &\lambda^2 \equiv (4/\widehat{\varepsilon})^3 \frac{m^2 S^2}{4r_m^2} \frac{T_i}{m_i \omega_{Bi}^2} \left[\frac{3}{4} + \frac{T_e}{T_i}\right] \ll 1 \end{split}$$

$$(42)$$

All local parameters in Eq. (42) need be evaluated at the gap location r_m defined by Eq. (3).

It is noteworthy that the exponent in the derived expression (42) for the damping rate is roughly the ratio of the TAE inner width to the short wavelength of the radiated KAW. The parametric dependence of the damping rate agrees with the result of Refs, [2–5], but the numerical factor in front of the exponent here is 1/12 instead of 1/8.

Expression (42) is suitable for benchmarking numerical codes in a limited but well-defined parameter range described in our work. That

parameter range may look challenging for the codes as happens often in extreme limiting cases. Yet, if successful, such limited testing would suggest that the codes are likely accurate under less challenging conditions.

It is desirable to generalize Eq. (42) to cover other relations between the shear and the aspect ratio and other modes that may exist within the gap, including the odd TAE mode. However, such generalization is less than straightforward. It goes beyond the scope of the present paper, the main goal of which is to offer a new technical approach to evaluating radiative damping with an opportunity for testing codes, albeit in a limited but well-defined parameter space. We believe that such generalization deserves a separate effort.

Submission

I think this is a wonderful fundamental paper perfectly fitting the scope of the Fundamental Plasma Physics journal.

CRediT authorship contribution statement

B.N. Breizman: Writing – original draft. **S.E. Sharapov:** Investigation.

Declaration of competing interest

The authors declare that they have no known competing financial interests or personal relationships that could have appeared to influence the work reported in this paper.

Acknowledgments

This work was supported by the U.S. Department of Energy Contract

Nos. DEFG02-04ER54742 and by the EPSRC Energy Programme [grant number EP/W006839/1].

Data availability

No data was used for the research described in the article.

References

- [1] M. Fitzgerald, S.E. Sharapov, P. Rodrigues, D. Borba, Predictive nonlinear studies of TAE-induced alpha-particle transport in the Q = 10 ITER baseline scenario, Nucl. Fusion 56 (2016) 112010.
- [2] J.W. Connor, et al., Non-ideal effects on TAE Stability, in: Proceed. of the 21st EPS Conference on Control. Fusion and Plasma Phys. Montpellier 18B, 1994, p. 616.
- [3] R. Nyqvist, S.E. Sharapov, Asymmetric radiative damping of low shear toroidal Alfvén eigenmodes, Phys. Plasmas. 19 (2012) 082517.
- [4] H.L. Berk, R.R. Mett, D.M. Lindberg, Arbitrary mode number boundary-layer theory for nonideal toroidal Alfvén modes, Phys. Fluids B 5 (1993) 3969.
- [5] G.Y. Fu, C.Z. Cheng, R. Budny, et al., Analysis of alpha particle-driven toroidal Alfven eigenmodes in Tokamak Fusion Test Reactor deuterium-tritium experiments, Phys. Plasmas. 3 (1996) 4036.
- [6] B.N. Breizman, S.E. Sharapov, Energetic particle drive for toroidicity-induced alfvén eigenmodes and kinetic toroidicity-induced Alfven eigenmodes in a lowshear tokamak, Plasma Phys. Control. Fusion 37 (1995) 1057.
- [7] J. Candy, B.N. Breizman, J.W. Van Dam, T. Ozeki, Multiplicity of low-shear toroidal Alfven eigenmodes, *Phys. Lett.* A 215 (1996) 299.
- [8] M.N. Rosenbluth, P.H. Rutherford, Excitation of Alfven waves by high-energy ions in a tokamak, Phys. Rev. Lett. 34 (1975) 1428.
- [9] R.R. Mett, S.M. Mahajan, Kinetic theory of toroidicity-induced Alfvén eigenmodes, Phys. Fluids B4 (1992) 2885.
- [10] J. Candy, M.N. Rosenbluth, Nonideal theory of toroidal Alfven eigenmodes, Phys. Plasmas. 1 (1994) 356.
- [11] M. Abramowitz, I. A Stegun, Handbook of Mathematical Functions With Formulas, Graphs, and Mathematical Tables-(NBS Applied Mathematics Series 55), DC US Govt Printing Office, Washington, 1964.